Dry reforming of methane over Zr- and Y-modified Ni/Mg/Al double-layered hydroxides

Katarzyna Świrk[1,2*], Maria Elena Gálvez[2], Monika Motak[1], Teresa Grzybek[1], Magnus Rønning[3], Patrick Da Costa [2]

[1] AGH University of Science and Technology, Faculty of Energy and Fuels, 30-059 Cracow, Poland
[2] Sorbonne Université, CNRS, Institut Jean le Rond d'Alembert, F-78210 Saint-Cyr-l'École, France
[3] Norwegian University of Science and Technology, Department of Chemical Engineering, N-7491 Trondheim, Norway

*Corresponding author:

Katarzyna Świrk

30 Mickiewicza Av., 30-059 Cracow, Poland

contact: +48 12 617 21 18, swirk@agh.edu.pl

2 place de la gare de ceinture, F-78210 Saint-Cyr-l'Ecole, France

contact: katarzyna.swirk@sorbonne-universite.fr

Abstract

Zr- and Y-promoted Ni/Mg/Al double-layered hydroxides were investigated in dry reforming of methane, DRM (10% CH_4, CH_4/CO_2=1, GHSV=20,000 h^{-1}) for the first time. Modification of the double-layered hydroxides with 5 wt% of zirconium and 0.4 wt% of yttrium resulted in the formation of ZrO_2-Y_2O_3 solid solution, which largely contributed to the enhancement of catalyst's stability with time-on-stream at 700 °C in DRM. Also, the modified catalyst demonstrated the limitation of the reverse WGS reaction, as confirmed by powder XRD due to the absence of the rhombohedral hydrotalcite structure.

Keywords: dry reforming of methane, hydrotalcite, zirconium promotion, yttrium promotion, syngas.

1. Introduction

In recent years much attention has been paid to the development of technologies for efficient carbon dioxide utilization. One of them is the dry reforming of methane (DRM), converting CO_2 and CH_4 into useful syngas through the following reaction: $CH_4 + CO_2 = 2CO + 2H_2$ (ΔH^o= 247 kJ/mol), where the H_2/CO product ratio of 1 is attractive for iron-based Fisher-Tropsch synthesis and production of oxygenated organic compounds [1–4]. Nickel based materials have been widely studied and were found to be promising alternatives to the expensive noble metals (e.g. Ru, Rh, Pt and Pd). However, their industrial application might be limited because of sintering of Ni nanoparticles and catalyst deactivation caused by carbon deposits [4–8]. The latter is the result of side reactions, mainly of the direct methane decomposition and the Boudouard reaction [1,3–5,9,10]. The catalyst preparation, including the support used and the addition of promoters, significantly influence the catalytic behavior, contributing to both catalytic activity and stability with time-on-stream.

Double-layered hydroxides, also known as hydrotalcites (HTs), show good properties as potential carriers due to their double layered structure and the presence of Mg^{2+} and Al^{3+} introduced by co-precipitation [3,11–15]. These cations can be partially substituted by the ions of the promoter, improving structural and catalytic properties of the material. Furthermore, Ni/Mg/Al hydrotalcites were found to be interesting catalysts for DRM, resulting in high catalytic activity at moderate operating temperatures [12,16]. It should be mentioned, however, that deactivation due to the formation of large amounts of graphitic carbon was observed [16]. The addition of Zr (3 wt%) to the catalyst composition resulted in the enhancement of stability, which originated from the suppression of direct methane decomposition. On the other hand, this improvement resulted in the decrease in activity, together with a lower H_2/CO product molar ratio. The catalyst modified with 5 wt% of Zr provided satisfactory activity results, but it suffered in terms of stability [16]. Thus, to find a

balance between activity and stability, stabilization of the catalytic system with zirconia (5 wt% phase) was considered. The properties of ZrO_2 can be tailored by the introduction of a cation with valence lower than 4+, e.g. Y^{3+} [9,17,18]. This results in the formation of defects in the crystal structure of zirconia, together with oxygen vacancies in its oxygen sub-lattice, which are known as beneficial in the minimization of carbon deposits [9,19–21]. The ZrO_2-Y_2O_3 solid solution was studied in the past in different reforming processes [20–23]. Bellido et al. [9] prepared different Y/Zr catalysts with a varying mole fraction of Y (4 to 12 mol%). The synthesized supported nickel 8YZ catalyst showed the best results in terms of activity and stability in the DRM [9]. The authors ascribed these properties to the increased formation of oxygen vacancies in the synthesized support. Recently, Vasiliades et al. [24] reported direct experimental evidence (use of transient isotopic experiments) for the participation of labile oxygen of CeO_2-ZrO_2 support in the DRM over NiCo/CeO_2-ZrO_2 for the first time.

Herein, Zr- and Y-promoted Ni/Mg/Al-hydrotalcite catalysts tested towards DRM are reported for the first time. Several important physicochemical properties of the added promoters were examined by several characterization techniques, such as XRF, N_2 sorption, TPR-H_2, TPD-CO_2, XRD, H_2 chemisorption, HRTEM and TGA.

2. Experimental

2.1. Catalysts preparation

Hydrotalcites were synthesized by the constant-pH co-precipitation method (pH=10±0.2) after using $Mg(NO_3)_2 \cdot 6H_2O$ (Sigma Aldrich, 99% pure), $Ni(NO_3)_2 \cdot 6H_2O$ (Sigma Aldrich, 98.5% pure) and $Al(NO_3)_3 \cdot 9H_2O$ (Fluka, 98% pure). The resulting precursors mixture was allowed to react for 24 h, and the obtained slurry was then filtered and washed with distilled water. A mixture of aqueous solutions of $ZrO(NO_3)_2 \cdot xH_2O$ (Sigma Aldrich, 99% pure) and $Y(NO_3)_3 \cdot 6H_2O$ (Aldrich, 99.8% pure) was used for the incipient wetness impregnation on the

dried Ni/Mg/Al solid support. The nominal amount of Zr was 5 wt%. The sample was promoted with 0.2, 0.4 or 0.6 wt% yttrium, corresponding to Y/Zr molar ratio of 0.2, 0.4 and 0.6, respectively. The final solid product was calcined in air at 550 °C for 5 h. The prepared catalysts were then labelled HT, HT/Zr, HT/ZrY0.2, HT/ZrY0.4, and HT/ZrY0.6, respectively.

2.2. Catalysts characterization

X-Ray Fluorescence analysis (Supermini200) was performed as described elsewhere [25], with the exception of the dilution ratio which was 1:40. N_2 sorption analysis (Micromeritics TriStar II 3020) was carried out at -195 °C preceded by sample degassing for 3 h at 110 °C before measurements. TPR-H_2 profiles (BEL Japan BELCAT-M) were obtained by using a thermal conductivity detector (TCD). 60 mg of each sample was outgassed in He at 100 °C for 2 h prior the analysis. Reduction was performed in the gas mixture of 5% H_2/Ar, while the temperature was increased at a heating rate of 7.5 °C/min up to 900 °C. TPD-CO_2 (BEL Japan BELCAT-M) was performed as described elsewhere [26] in order to determine surface basicity. XRD (PANalytical-Empyrean) was carried out using a CuKα (λ=0.15406 nm) radiation source. The average crystallite size of Ni° and the average primary crystal size of ZrO_2 were determined by the Scherrer equation. Nickel dispersion on reduced samples was measured by H_2 chemisorption (Micromeritics ASAP 2020) at 40 ºC using pure H_2 flow of 50 ml/min. Prior the experiments, all samples were reduced in situ at 900 ºC. High Resolution Transmission Electron Microscopy coupled with Emission Dispersive Spectroscopy (JEOL JEM-2010) was performed for the samples firstly dispersed in ethanol solution by ultrasonication and then placed as suspensions on copper grids. Thermogravimetric analyses were carried out for spent catalysts in a Netzsch STA 449C Jupiter TGA apparatus under oxidizing atmosphere (air) with a total flow of 100 cm^3/min.

2.3. Catalytic performance tests

Dry reforming of methane tests were performed in a fixed-bed reactor with a K-type thermocouple to control the temperature in the catalytic bed. An electric furnace was used for heating. Prior to the DRM reaction, the catalyst sample was reduced in situ at 900 °C for 1 h with 5% H_2/Ar gas mixture (flow 50 cm^3/min). Then, catalytic experiments were performed in the range of 850-600 °C with a temperature step of 50 °C and stay for 30 min in the DRM reaction at each temperature. For the stability test, the catalysts were kept for 5 h at 700 °C. For each catalytic test, the total reactant flow was set to 100 cm^3/min of $CH_4/CO_2/Ar$=1/1/8 (10%CH_4/10%CO_2/80%Ar), corresponding to a GHSV=20,000 h^{-1}. The outlet gas composition was analyzed by gas chromatography (490 Varian Micro-GC).

3. Results and discussion

3.1. Catalysts characterization

Elemental analysis of the calcined materials revealed Ni content within 15-20 wt% (Table 1). During the synthesis step, 5 wt% of Zr and Al^{3+}/Zr^{4+}=5.0 nominal values were used. However, the content of Zr and the Al^{3+}/Zr^{4+} ratio was 2.5, 2.7, 2.6, 2.4 wt% and 15.3, 14.1, 15.9, 16.1 for HT/Zr, HT/ZrY0.2, HT/ZrY0.4 and HT/ZrY0.6, respectively. These results show that Zr was only partially incorporated into the hydrotalcite structure, similarly as described by Dębek et al. [16]. The yttrium content was found the same as the nominal value, i.e. 0.2, 0.4 and 0.6 wt%.

The modification of HT with zirconium caused a slight decrease of the specific surface area (S_{BET}), ca. 105 m^2/g for HT/Zr, whereas 120 m^2/g was obtained for the unpromoted HT (Table 1). No significant changes of the textural properties were observed after modification with yttrium. S_{BET} had the same value of 107 m^2/g for each of the Y-modified catalysts. The

specific pore volume of mesopores varied from 0.5 to 0.6 cm^3/g, and pore diameters from 18 to 19 nm in all prepared catalysts.

TPR-H_2 profiles of the reduced materials showed a wide reduction peak starting from 600 °C and centered at ca. 850 °C (Fig. 1). This reduction peak corresponds to NiO incorporated within the structure of periclase [16]. Zr and Zr/Y addition resulted in a rightward shift of the peak maximum of the wide peak, together with lower H_2 consumption, and these features reflect the decrease of reducibility of the solid material. The samples modified with 0.2% and 0.6% of Y show a peak maximum at ~ 847 °C. A more pronounced shift is observed in the Y0.4-promoted catalyst, which suggests stronger interactions of Ni particles with the support [27]. At lower temperatures, shoulders were registered, where the one observed at 385 °C in HT catalyst is assigned to weakly-bonded NiO [2,28]. After modification with Zr the doublet at 330 and 394 °C observed is probably due to the presence of bulk NiO [29]. The subsequent modification with 0.2 and 0.6 wt% yttrium resulted in the stabilization of NiO species. This was not observed in the HT/ZrY0.4 catalyst, where only one reduction peak centered at 400 °C is registered, indicating the absence of bulk NiO.

TPD-CO_2 results are presented in Table 1, where changes among weak, medium and strong basic sites are observed. Their distribution varies with the solid catalysts modifications. In particular, promotion with Zr decreased the number density of strong surface basic sites for medium and weak. After further promotion with yttrium, the strong sites have been expanded as compared to those of Y-free solid, giving the highest proportion for the Y0.2 sample, ca. 57%. However, promotion with Y0.6 resulted in the decrease of strong and an increase of medium surface basic sites. The latter kind of basic sites was reported to play a significant role in DRM [30]. Also, the total basicity decreased after promotion of HT material, i.e. 107, 72, 84, 85, 79 μmol/g for HT, HT/Zr, HT/ZrY0.2, HT/ZrY0.4, HT/ZrY0.6, respectively. All the calculated data of basicity are presented in Fig. 1S in ESI.

XRD patterns of the reduced samples are presented in Fig. 2A. Characteristic reflections of periclase mixed oxides, metallic nickel Ni^o and ZrO_2 are observed [3,8,27]. Additionally, XRD analysis revealed the possible presence of magnesium-zirconium oxide and aluminum-zirconium oxide, indicating strong interactions of Zr with the support. No separate phase of yttrium oxide is observed, probably due to its low content, which makes it undetectable by XRD. However, Y-doping with a higher amount of 0.4 wt% resulted in a shift of the reflection at 2θ, ca. 30°, towards lower Bragg angles, which suggests an increase in the interlayer distance of zirconia, as reported elsewhere [9,17,31–33]. Yttrium ions can enter the zirconia crystal lattice, resulting in the formation of ZrO_2-Y_2O_3 solid solution, and this is further confirmed by HRTEM analysis (see Fig. 4). The size of ZrO_2 primary crystallites (calculated from the Scherrer equation using the 2θ diffraction peak at 31°), was 11 nm for the Zr-containing materials. This is in agreement with the study of Asencios et al. [19], where ZrO_2 crystallites with non-variable size were detected by XRD. Moreover, the calculated mean Ni crystallite size (at 2θ ca. 52°) was found to be practically the same for all the studied catalysts. No shift of Ni° reflections was observed among the tested materials, indicating the absence of either Y_2O_3-NiO or ZrO_2-NiO solid solution [21].

The dispersion of nickel for the HT material slightly decreased after modification with zirconium, i.e. 8.9% versus 7.8% (Table 1). After further promotion with yttrium an increase of Ni dispersion was observed, showing the highest value for HT/ZrY0.6 catalyst. The increase of dispersion after Y-promotion was also reported [25,28,34,35].

3.2. Catalytic performance in DRM

Fig. 3A presents catalytic results of the DRM in terms of CH_4 and CO_2 conversion and H_2/CO product ratio in the 600-850^{o}C range. All catalysts are found active under the tested DRM conditions, showing within experimental error, a similar catalytic performance, with the

exception of HT/ZrY0.2 catalyst, which shows lower conversions. The CO_2 conversion is higher than that of CH_4, indicating the occurrence of side reactions, mainly of RWGS, which is in agreement with the lower than unity H_2/CO ratio [4,12,21].

Stability tests were carried out at 700 ºC for 300 min (5 h) (Fig. 3B). For the HT/ZrY0.4 catalyst, higher reactant conversions are observed in comparison to HT/Zr. For the latter, the reactant conversion values are constantly increasing with TOS during the first 75 min of DRM. This may suggest unstable performance of the Zr-impregnated catalyst, and a possible enhancement of the stability due to yttrium addition since HT/ZrY0.4 did not show such behavior. Moreover, lower catalytic performance is obtained for the unmodified material, where after 75 min of DRM conversions of CH_4 and CO_2 of 72.7% and 74.7%, respectively, are observed. This is in contrast to the results reported by Dębek et al. [2,16]. The latter authors studied Ni-based hydrotalcites at 550 ºC (CH_4/CO_2=1, GHSV=20,000 h^{-1}). The unpromoted catalyst HT showed selectivity towards direct decomposition of CH_4, which is considered as boosting of the H_2/CO ratio due to the excess hydrogen (Fig. 3A). Also, the HT catalyst shows higher activity compared to the Zr-modified materials (3-10 wt%). A similar trend was observed in other activity tests carried out at 650 and 750 ºC over the HNi and HNiZr3 samples. Thus, in this study, it is shown that impregnation of Ni/Mg/Al double-layered hydroxides with Zr (5 wt%) and Y (0.4 wt%) not only enhanced the stability in DRM but also improved the catalyst's activity as compared to the unmodified Ni-based catalyst.

The differences in catalysts stability could have been related with the improvement of Ni dispersion (H_2 chemisorption) and changes in basicity (TPD-CO_2). Both are known to contribute to better catalytic performance [26,36,37].

Surprisingly, the formation of ZrO_2-Y_2O_3 solid solution (XRD) did not lead to an increased reducibility of the Y-loaded materials, as previously reported by several authors [20,21,35]. The increase of H_2 uptake could explain the possible formation of oxygen

vacancies, which may endorse an increase in the rate of carbon deposit elimination in the vicinity of active nickel, e.g. via the reverse Boudouard reaction (CO_2 + C = 2 CO) [38]. Furthermore, the distinctive reducibility behavior observed in the HT/ZrY0.4 catalyst, i.e. stronger Ni interactions with the support and the lack of bulk NiO are noted. It might be suggested that the ZrO_2-Y_2O_3 phase, located on the surface of the catalyst, is largely able to lead to the reduction of the surface NiO by decreasing the formation of bulk NiO. This may contribute to the better stability and less coke formation.

3.3. Characterization of spent catalysts

Fig. 2B shows XRD patterns of the spent catalysts after DRM activity tests. Apart from the Ni°, ZrO_2 and periclase reflections, the ones resulting from hydrotalcite (HT) are also observed. This indicates a partial regeneration of the support during DRM, which may be observed in hydrotalcite-derived materials in the presence of water [27]. Thus, it may be suggested that one of the side reactions, such as RWGS (CO_2 + H_2 = CO + H_2O), had a significant involvement in the tested catalysts towards DRM. Only the unmodified material, and the one with Zr and Y 0.4 wt% did not reveal the presence of double layered hydroxides. Mean crystallite sizes of the metallic Ni° are summarized in Table 1, which vary from 8 to 5 nm. For all catalysts, the crystallite Ni° sizes after DRM tests (aged catalysts) are slightly smaller than those obtained for the reduced samples, result which might be due to Ni re-dispersion upon continuous reduction and oxidation of nickel [39]. A similar phenomenon was previously observed in DLHs [2,40]. In this study, the smaller Ni° sizes are further confirmed by HRTEM analysis (Fig. 4).

HRTEM images of the spent catalysts are shown in Fig. 4. On the left-hand side, micrographs of HT/Zr catalyst are presented which show randomly-distributed Ni particles, between 4 to 18 nm. Carbon nanotubes formed after DRM and related to the presence of

nickel particles are also registered in this material. The results of EDS analysis show the existence of Ni and Zr. A detailed examination showed the presence of ZrO_2 aggregates with particle size in the range of 6-11 nm, and interplanar distance in the 0.29 - 0.30 nm range. No ZrO_2-NiO solid solution was registered. On the right-hand side of Fig. 4, images of the spent HT/ZrY0.4 catalyst are presented. The shown histograms of Ni particles evidence a decrease in the average Ni size compared to HT/Zr. For the HT/ZrY0.4 sample, the EDS analysis revealed the presence of zirconium in the direct vicinity of yttrium. ZrO_2-Y_2O_3 solid solution (with d-spacing of 0.29, 0.28, 0.30 nm) was observed in the form of aggregates. For both spent catalysts, graphitic carbon was registered with an interlayer distance of 0.32 nm [41,42]. For the HT/Zr catalyst micrographs of graphitic carbon are shown in ESI (Fig. 2S). Also, Ni particles with average d-spacing of 0.20 nm, corresponding to the (111) plane, and encapsulated by carbon layers was reported [43].

TGA analysis of the spent materials (Fig. 3S, ESI) probed for the lowest mass loss for the HT/ZrY0.4 catalyst, indicating the relatively low carbon formation rate, and thus a better stability compared to the other catalysts. The highest mass loss was observed for the HT/ZrY0.2 and HT/ZrY0.6 catalysts, the former showing the lowest conversions in DRM activity, whereas the latter showing relatively high conversions. Furthermore, the amount of carbon deposited is high as compared to the studies reported, where essentially no coke was detected after 170 h of DRM [44].

4. Conclusions

In this work, Ni/Mg/Al hydrotalcites (HT) were modified with Zr and Y (0.2-0.6 wt%) and tested towards the DRM. Dry impregnation of HT with Zr and Y promoters resulted in the partial incorporation of ZrO_2 and Y_2O_3, and their interaction with the periclase support. A

decrease in reducibility, together with lower H_2 consumption and stronger interactions of nickel with the modified-HT support were observed.

The material promoted with Zr and 0.4 wt% of Y was catalytically active and stable in DRM (10% CH_4, CH_4/CO_2=1) at 700ºC. It showed structural resistance to the products of the RWGS side reaction, as supported by the absence of hydrotalcite reflections in the XRD patterns of the spent catalyst. Moreover, the improvement of catalyst stability was clearly shown at 700 ºC for 5 h of TOS, where the HT/ZrY0.4 catalyst was more stable than the Y-free material. The observed better stability may have arisen from favorable changes in the distribution of surface basic sites, reduction of bulk NiO and improved Ni dispersion.

Acknowledgments

K. Świrk acknowledges the French Embassy in Poland for her PhD grant at Sorbonne Université, and InnoEnergy PhD School for financial support. The KinCat Catalysis Group at NTNU is gratefully acknowledged for the possibility to conduct this research during an Erasmus+ traineeship of K. Świrk. T. Grzybek and M. Motak thank AGH grant 11.11.210.373. Thanks to Patricia Beaunier (Sorbonne Université) for the HRTEM measurements.

References

[1] E. Alper, O. Yuksel Orhan, CO_2 utilization: Developments in conversion processes, Petroleum. 3 (2017) 109–126. doi:10.1016/j.petlm.2016.11.003.

[2] R. Dębek, M. Motak, M.E. Galvez, T. Grzybek, P. Da Costa, Influence of Ce/Zr molar ratio on catalytic performance of hydrotalcite-derived catalysts at low temperature CO_2 methane reforming, Int. J. Hydrogen Energy. 42 (2017) 1–12. doi:10.1016/j.ijhydene.2016.12.121.

[3] R. Dębek, M. Motak, M.E. Galvez, P. Da Costa, T. Grzybek, Catalytic activity of hydrotalcite-derived catalysts in the dry reforming of methane: on the effect of Ce promotion and feed gas composition, React. Kinet. Mech. Catal. 121 (2017) 185–208. doi:10.1007/s11144-017-1167-1.

[4] D. Pakhare, J. Spivey, A review of dry (CO_2) reforming of methane over noble metal catalysts, Chem. Soc. Rev. 43 (2014) 7813–7837. doi:10.1039/C3CS60395D.

[5] O. Muraza, A. Galadima, A review on coke management during dry reforming of methane, Int. J. Energy Res. 39 (2015) 1196–1216. doi:10.1002/er.

[6] J. Sehested, J.A.P. Gelten, S. Helveg, Sintering of nickel catalysts: Effects of time, atmosphere, temperature, nickel-carrier interactions, and dopants, Appl. Catal. A Gen. 309 (2006) 237–246. doi:10.1016/j.apcata.2006.05.017.

[7] S. Kawi, Y. Kathiraser, J. Ni, U. Oemar, Z. Li, E.T. Saw, Progress in synthesis of highly active and stable nickel-based catalysts for carbon dioxide reforming of methane, ChemSusChem. 8 (2015) 3556–3575. doi:10.1002/cssc.201500390.

[8] W. Li, Z. Zhao, G. Wang, Modulating morphology and textural properties of ZrO_2 for supported Ni catalysts towards dry reforming of methane, AIChE J. 63 (2017) 2900–2915. doi:10.1002/aic.

[9] J.D.A. Bellido, E.M. Assaf, Effect of the Y_2O_3-ZrO_2 support composition on nickel catalyst evaluated in dry reforming of methane, Appl. Catal. A Gen. 352 (2009) 179–187. doi:10.1016/j.apcata.2008.10.002.

[10] R. Zanganeh, M. Rezaei, A. Zamaniyan, Dry reforming of methane to synthesis gas on NiO-MgO nanocrystalline solid solution catalysts, Int. J. Hydrogen Energy. 38 (2013) 3012–3018. doi:10.1016/j.ijhydene.2012.12.089.

[11] F. Cavani, F. Trifirò, A. Vaccari, Hydrotalcite-type anionic clays: Preparation, properties and applications., Catal. Today. 11 (1991) 173–301. doi:10.1016/0920-5861(91)80068-K.

[12] R. Dębek, M. Motak, T. Grzybek, M. Galvez, P. Da Costa, A short review on the catalytic activity of hydrotalcite-derived materials for dry reforming of methane, Catalysts. 7 (2017) 32–57. doi:10.3390/catal7010032.

[13] A. Bhattacharyya, V.W. Chang, D.J. Schumacher, CO_2 reforming of methane to syngas I: Evaluation of hydrotalcite clay-derived catalysts, Appl. Clay Sci. 13 (1998) 317–328. doi:10.1016/S0169-1317(98)00030-1.

[14] H.-Y. Zeng, X. Deng, Y.-J. Wang, K.-B. Liao, Preparation of Mg-Al hydrotalcite by urea method and its catalytic activity for transesterification, AIChE J. 55 (2009) 1229–1235. doi:10.1002/aic.

[15] A.I. Tsyganok, M. Inaba, T. Tsunoda, S. Hamakawa, K. Suzuki, T. Hayakawa, Dry reforming of methane over supported noble metals: A novel approach to preparing catalysts, Catal. Commun. 4 (2003) 493–498. doi:10.1016/S1566-7367(03)00130-4.

[16] R. Dębek, M. Motak, M.E. Galvez, T. Grzybek, P. Da Costa, Promotion effect of zirconia on Mg(Ni,Al)O mixed oxides derived from hydrotalcites in CO_2 methane reforming, Appl. Catal. B Environ. (2018) 36–46. doi:10.1016/j.apcatb.2017.06.024.

[17] X. Xu, X. Wang, Fine tuning of the sizes and phases of ZrO_2 nanocrystals, Nano Res. 2

(2009) 891–902. doi:10.1007/s12274-009-9092-x.
[18] A. Białas, T. Kondratowicz, M. Drozdek, P. Kuśtrowski, Catalytic combustion of toluene over copper oxide deposited on two types of yttria-stabilized zirconia, Catal. Today. 257 (2015) 144–149. doi:10.1016/j.cattod.2015.01.005.
[19] Y.J.O. Asencios, F.C.F. Marcos, J.M. Assaf, E.M. Assaf, Oxidative-reforming of methane and partial oxidation of methane reactions over $NiO/PrO_2/ZrO_2$ catalysts : Effect of nickel content, Brazilian J. Chem. Eng. 33 (2016) 627–636.
[20] J.D.A. Bellido, E.Y. Tanabe, E.M. Assaf, Carbon dioxide reforming of ethanol over Ni/Y_2O_3-ZrO_2 catalysts, Appl. Catal. B Environ. 90 (2009) 485–488. doi:10.1016/j.apcatb.2009.04.009.
[21] Y.J.O. Asencios, C.B. Rodella, E.M. Assaf, Oxidative reforming of model biogas over NiO-Y_2O_3-ZrO_2 catalysts, Appl. Catal. B Environ. 132–133 (2013) 1–12. doi:10.1016/j.apcatb.2012.10.032.
[22] K. Dong-Hee, L.; Kwang-Seo, C.; Hyo-Sub K.; Chu-Sik, P.; Young-Ho, Syngas and hydrogen production via stepwise methane reforming over Cu-ferrite/YSZ, Int. J. Energy Res. 31 (2007) 1522–1530. doi:10.1002/er.
[23] C. Resini, M. Concepción Herrera Delgado, S. Presto, L.J. Alemany, P. Riani, R. Marazza, G. Ramis, G. Busca, Yttria-stabilized zirconia (YSZ) supported Ni-Co alloys (precursor of SOFC anodes) as catalysts for the steam reforming of ethanol, Int. J. Hydrogen Energy. 33 (2008) 3728–3735. doi:10.1016/j.ijhydene.2008.04.044.
[24] M.A. Vasiliades, P. Djinović, A. Pintar, J. Kovač, A.M. Efstathiou, The effect of CeO_2-ZrO_2 structural differences on the origin and reactivity of carbon formed during methane dry reforming over $NiCo/CeO_2$-ZrO_2 catalysts studied by transient techniques, Catal. Sci. Technol. 7 (2017) 5422–5434. doi:10.1039/c7cy01009e.
[25] K. Świrk, M.E. Gálvez, M. Motak, T. Grzybek, M. Rønning, P. Da Costa, Syngas production from dry methane reforming over yttrium-promoted nickel-KIT-6 catalysts, Int. J. Hydrogen Energy. (2018). doi:10.1016/j.ijhydene.2018.02.164.
[26] R. Dębek, M. Radlik, M. Motak, M.E. Galvez, W. Turek, P. Da Costa, T. Grzybek, Ni-containing Ce-promoted hydrotalcite derived materials as catalysts for methane reforming with carbon dioxide at low temperature - On the effect of basicity, Catal. Today. 257 (2015) 59–65. doi:10.1016/j.cattod.2015.03.017.
[27] R. Dębek, M. Motak, D. Duraczyska, F. Launay, M.E. Galvez, T. Grzybek, P. Da Costa, Methane dry reforming over hydrotalcite-derived Ni–Mg–Al mixed oxides: the influence of Ni content on catalytic activity, selectivity and stability, Catal. Sci. Technol. 6 (2016) 6705–6715. doi:10.1039/C6CY00906A.
[28] K. Świrk, M.E. Gálvez, M. Motak, T. Grzybek, M. Rønning, P. Da Costa, Yttrium promoted Ni-based double-layered hydroxides for dry methane reforming, J. CO2 Util. 27 (2018) 247–258. doi:10.1016/j.jcou.2018.08.004.
[29] A. Kadkhodayan, A. Brenner, Temperature-programmed reduction and oxidation of metals supported on γ-alumina, J. Catal. 117 (1989) 311–321. doi:10.1016/0021-9517(89)90342-4.
[30] H. Liu, D. Wierzbicki, R. Debek, M. Motak, T. Grzybek, P. Da Costa, M.E. Gálvez, La-promoted Ni-hydrotalcite-derived catalysts for dry reforming of methane at low temperatures, Fuel. 182 (2016) 8–16. doi:10.1016/j.fuel.2016.05.073.
[31] T. Götsch, W. Wallisch, M. Stöger-Pollach, B. Klötzer, S. Penner, From zirconia to yttria: Sampling the YSZ phase diagram using sputter-deposited thin films, AIP Adv. 6 (2016). doi:10.1063/1.4942818.
[32] M.B. Pomfret, C. Stoltz, B. Varughese, R.A. Walker, Structural and compositional characterization of yttria-stabilized zirconia: Evidence of surface-stabilized, low-valence metal species, Anal. Chem. 77 (2005) 1791–1795. doi:10.1021/ac048600u.

[33] R.P. Ingel, D.L. Iii, Lattice Parameters and Density for Y_2O_3-Stabilized ZrO_2, J. Am. Ceram. Soc. 69 (1986) 325–332. doi:10.1111/j.1151-2916.1986.tb04741.x.
[34] X. Huang, G. Xue, C. Wang, N. Zhao, N. Sun, W. Wei, Y. Sun, Highly stable mesoporous $NiO–Y_2O_3–Al_2O_3$ catalysts for CO_2 reforming of methane: effect of Ni embedding and Y_2O_3 promotion, Catal. Sci. Technol. 6 (2016) 449–459. doi:10.1039/C5CY01171J.
[35] B. Li, S. Zhang, Methane reforming with CO_2 using nickel catalysts supported on yttria-doped SBA-15 mesoporous materials via sol-gel process, Int. J. Hydrogen Energy. 38 (2013) 14250–14260. doi:10.1016/j.ijhydene.2013.08.105.
[36] H. Seo, Recent scientific progress on developing supported Ni catalysts for dry (CO_2) reforming of methane, Catalysts. 8 (2018) 110–128. doi:10.3390/catal8030110.
[37] R. Zhang, G. Xia, M. Li, Y. Wu, H. Nie, D. Li, Effect of support on the performance of Ni-based catalyst in methane dry reforming, J. Fuel Chem. Technol. 43 (2015) 1359–1365. doi:10.1016/S1872-5813(15)30040-2.
[38] W. Wang, S.M. Stagg-Williams, F.B. Noronha, L. V. Mattos, F.B. Passos, Partial oxidation and combined reforming of methane on Ce-promoted catalysts, Catal. Today. 98 (2004) 553–563. doi:10.1016/j.cattod.2004.09.009.
[39] T. Nakayama, M. Arai, Y. Nishiyama, Dispersion of nickel particles supported on alumina and silica in oxygen and hydrogen, J. Catal. 87 (1984) 108–115. doi:10.1016/0021-9517(84)90173-8.
[40] D. Li, K. Nishida, Y. Zhan, T. Shishido, Y. Oumi, T. Sano, K. Takehira, Sustainable Ru-doped Ni catalyst derived from hydrotalcite in propane reforming, Appl. Clay Sci. 43 (2009) 49–56. doi:10.1016/j.clay.2008.07.014.
[41] O. V. Kharissova, B.I. Kharisov, Variations of interlayer spacing in carbon nanotubes, RSC Adv. 4 (2014) 30807–30815. doi:10.1039/C4RA04201H.
[42] H. Li, X. He, Z. Kang, H. Huang, Y. Liu, J. Liu, S. Lian, C.H.A. Tsang, X. Yang, S.T. Lee, Water-soluble fluorescent carbon quantum dots and photocatalyst design, Angew. Chemie - Int. Ed. 49 (2010) 4430–4434. doi:10.1002/anie.200906154.
[43] C.T. Wirth, S. Hofmann, J. Robertson, State of the catalyst during carbon nanotube growth, Diam. Relat. Mater. 18 (2009) 940–945. doi:10.1016/j.diamond.2009.01.030.
[44] J.W. Han, C. Kim, J.S. Park, H. Lee, Highly coke-resistant Ni nanoparticle catalysts with minimal sintering in dry reforming of methane, ChemSusChem. 7 (2014) 451–456. doi:10.1002/cssc.201301134.

List of Figures captions:

Fig. 1. TPR-H_2 profiles recorded over hydrotalcites (HT) modified with Zr and Zr/Y. *(Total hydrogen consumption is given in brackets).

Fig. 2. XRD patterns recorded over the catalysts reduced at 900°C (A) and the spent catalysts after DRM (B).

Fig. 3. DRM activity performance tests (CH_4- and CO_2-conversion, H_2/CO gas product ratio) conducted over Zr,Y-promoted Ni/Mg/Al hydrotalcites; activity performance tests were conducted in the 600-850ºC range (A), and stability tests at 700 °C for 300 min (B).

Fig. 4. HRTEM micrographs with EDS analysis performed on the spent HT/Zr and HT/ZrY0.4 catalysts.

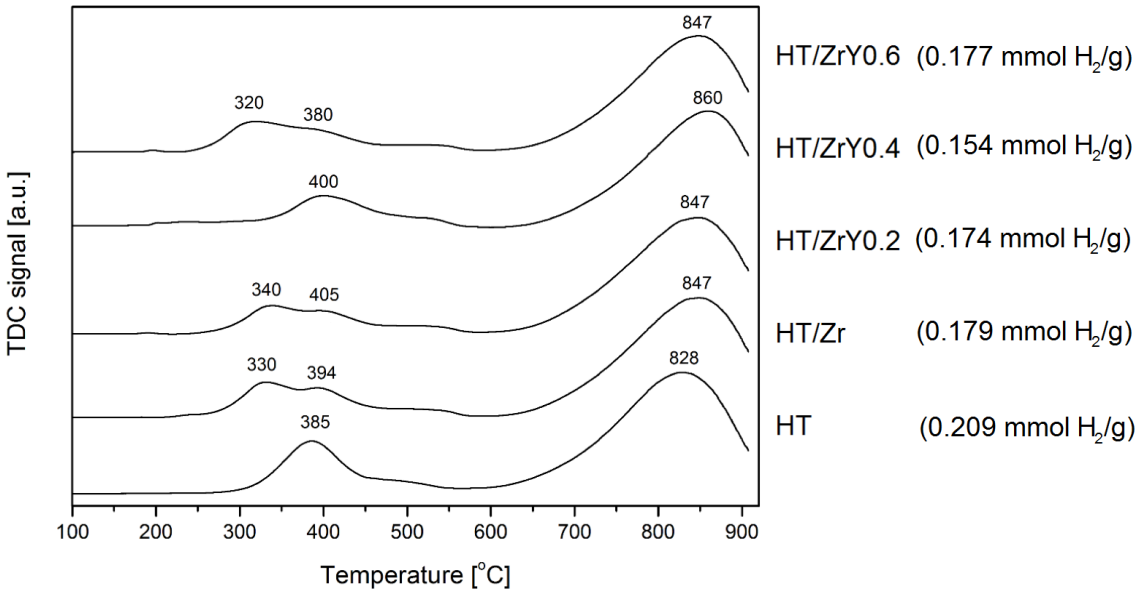
TDC signal [a.u.]
Temperature [°C]
100
200
300
400
500
600
700
800
900
847
320
380
860
400
847
340
405
847
330
394
828
385
HT/ZrY0.6 (0.177 mmol H2/g)
HT/ZrY0.4 (0.154 mmol H2/g)
HT/ZrY0.2 (0.174 mmol H2/g)
HT/Zr (0.179 mmol H2/g)
HT (0.209 mmol H2/g)

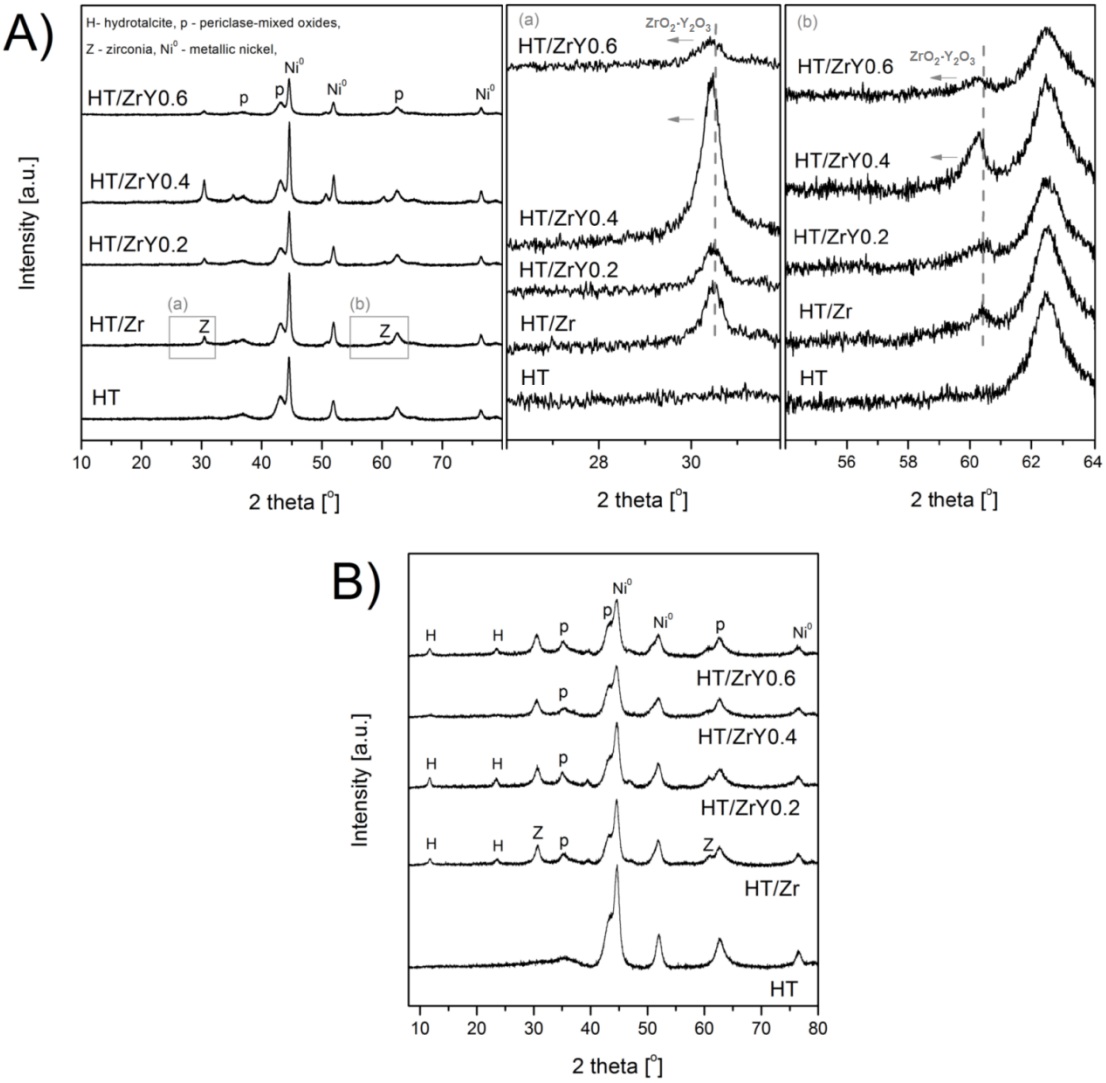
A)
H- hydrotalcite, p - periclase-mixed oxides,
Z - zirconia, Ni0 - metallic nickel,
HT/ZrY0.6
HT/ZrY0.4
HT/ZrY0.2
HT/Zr
HT
Intensity [a.u.]
2 theta [°]
(a)
(b)
ZrO2-Y2O3
B)

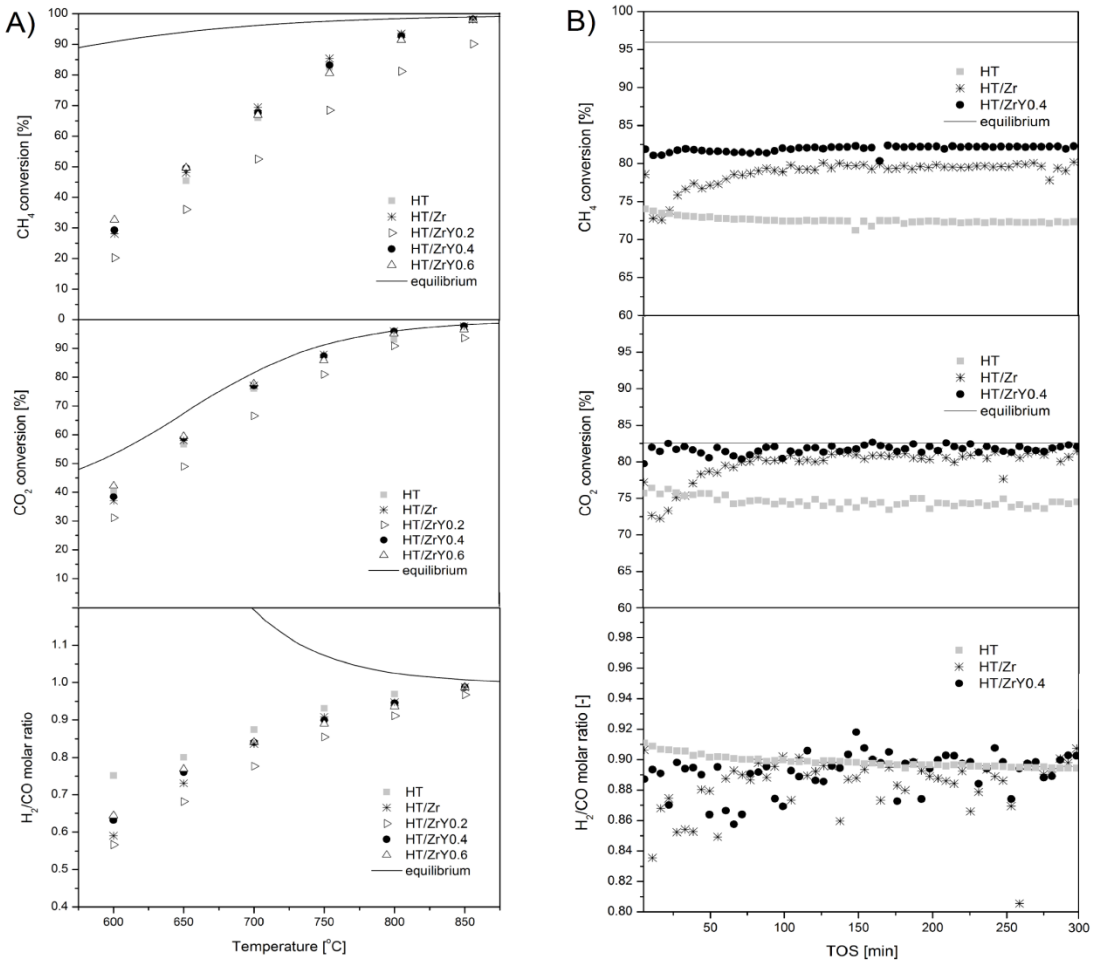
A)
CH4 conversion [%]
CO2 conversion [%]
H2/CO molar ratio
HT
HT/Zr
HT/ZrY0.2
HT/ZrY0.4
HT/ZrY0.6
equilibrium
Temperature [°C]
B)
CH4 conversion [%]
CO2 conversion [%]
H2/CO molar ratio [-]
HT
HT/Zr
HT/ZrY0.4
equilibrium
TOS [min]

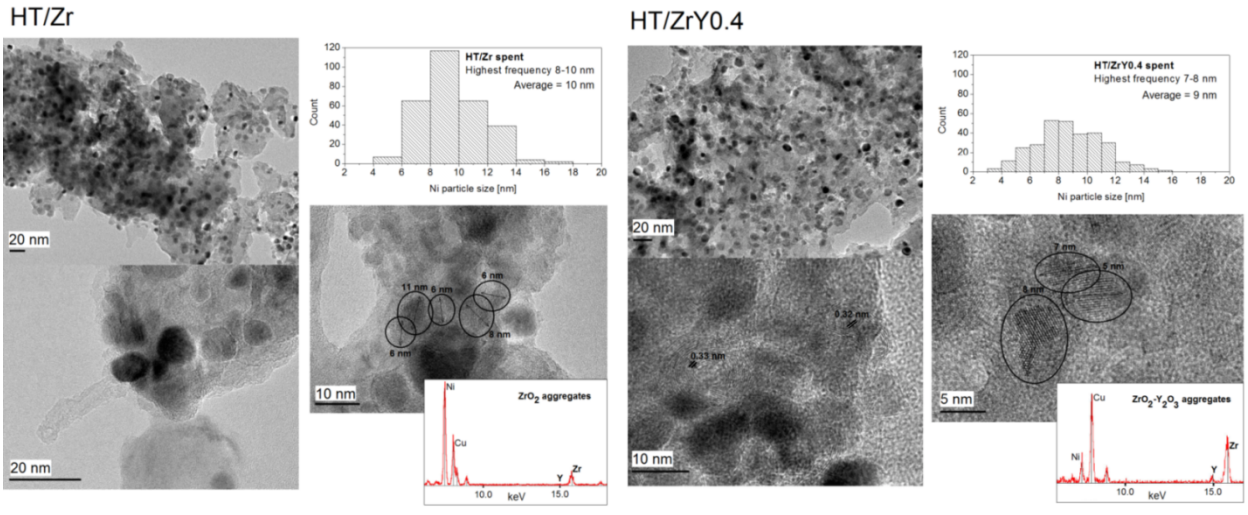
HT/Zr
20 nm
20 nm
HT/Zr spent
Highest frequency 8-10 nm
Average = 10 nm
Count
Ni particle size [nm]
10 nm
ZrO2 aggregates
Ni
Cu
Y
Zr
keV
HT/ZrY0.4
20 nm
10 nm
HT/ZrY0.4 spent
Highest frequency 7-8 nm
Average = 9 nm
5 nm
ZrO2-Y2O3 aggregates

List of Tables Captions

Table 1. Elemental composition (XRF), textural properties (N_2 sorption), basicity (TPD-CO_2), Ni° crystallite size (XRD) and Ni dispersion (H_2 chemisorption) of hydrotalcite-derived catalysts modified with zirconium and yttrium. Nominal values are presented in brackets.

Table 1. Elemental composition (XRF), textural properties (N_2 sorption), basicity (TPD-CO_2), Ni° crystallite size (XRD) and Ni dispersion (H_2 chemisorption) of hydrotalcite-derived catalysts modified with zirconium and yttrium. Nominal values are presented in brackets.

Catalyst	Elemental composition of the calcined materials							Textural properties of calcined materials			Basic sites				Ni° crystallite size		Ni dispersion
	Mg [wt.%]	Al [wt.%]	Ni [wt.%]	Zr [wt.%]	Y [wt.%]	Ni^{2+}/Mg^{2+} molar ratio	Al^{3+}/Zr^{4+} molar ratio	S_{BET} [m^2/g] [1)]	V_p [cm^3/g] [2)]	d_p [nm] [3)]	Weak [%]	Medium [%]	Strong [%]	Total [µmol/g]	Reduced samples [nm] [4)]	Spent samples [nm] [4)]	Reduced samples [%]
HT	30	12	20	-	-	0.29 (0.33)	-	120	0.6	19	16	41	43	107	8	5	8.9
HT/Zr	31	12	16	2.5 (5.0)	-	0.21 (0.33)	15.3 (5.0)	105	0.6	18	22	49	29	72	10	9	7.8
HT/ZrY0.2	30	11	18	2.7 (5.0)	0.2 (0.2)	0.24 (0.33)	14.1 (5.0)	107	0.6	18	13	30	57	84	10	8	9.8
HT/ZrY0.4	32	12	15	2.6 (5.0)	0.4 (0.4)	0.19 (0.33)	15.9 (5.0)	107	0.5	19	20	42	38	85	11	8	10.0
HT/ZrY0.6	32	12	15	2.4 (5.0)	0.6 (0.6)	0.20 (0.33)	16.1 (5.0)	107	0.5	18	20	58	22	79	10	8	11.1

[1)] specific surface areas calculated from the BET equation

[2)] mesopore volumes derived from the BJH desorption isotherm

[3)] pore size distribution obtained from the BJH desorption isotherm

[4)] derived from the Scherrer equation at $2\theta=52°$

Supplementary Materials

Characterization

Fig. 1S presents TPD-CO_2 profiles.

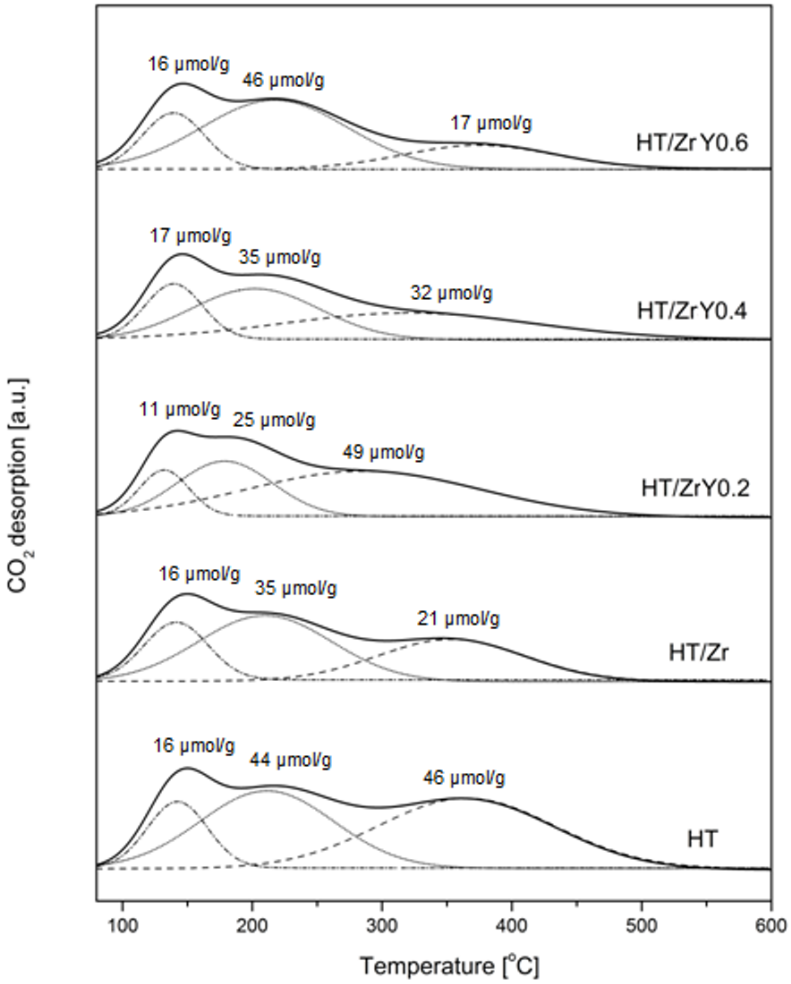

Fig. 1S TPD-CO_2 results of Zr,Y-modified hydrotalcites.

Fig. 2S shows HRTEM micrographs of the spent HT/Zr catalyst. Also, the metallic Ni particle with 0.20 nm spacing, corresponding to (111) plane, was encapsulated by the carbon layers.

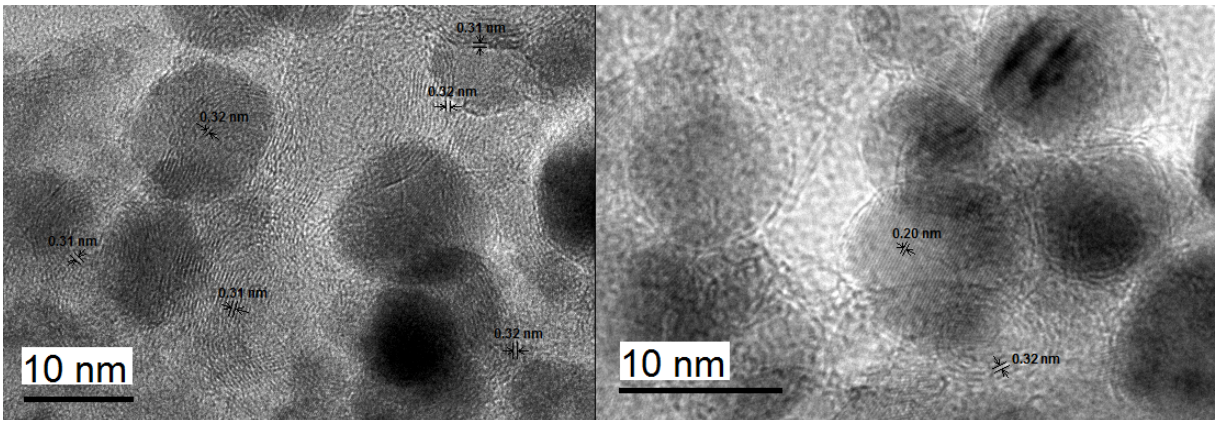

Fig. 2S HRTEM of HT/Zr spent catalyst: Formed carbon.

TGA analysis of the spent catalysts showed the lowest mass loss for the HT/ZrY0.4, indicating relatively low carbon formation, and thus better stability as compared to the other tested catalysts (Fig. 3S). The highest mass loss was observed for HT/ZrY0.2 and HT/ZrY0.6 catalysts, the former showing the lowest conversions in DRM activity tests, and the latter showing relatively high conversions.

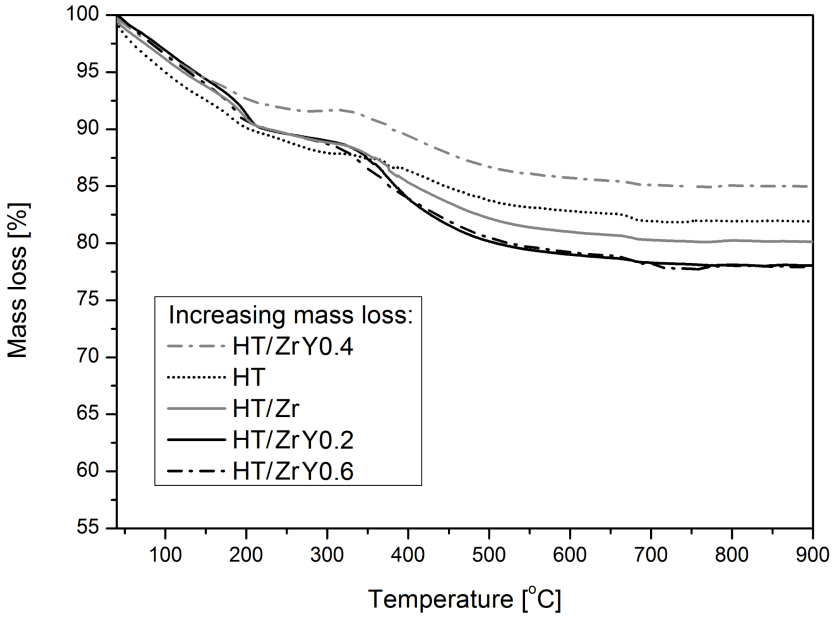

Fig. 3S TGA curves of Zr,Y-modified hydrotalcites after DRM tests.